UCRL-CR-125780
S/C-B264110

# Solution of Dynamic Contact Problems by Implicit/Explicit Methods

**Matthew W. Salveson**
**Professor Robert L. Taylor**
**Department of Civil and Environmental Engineering**
**University of California, Berkeley**

**October 14, 1996**

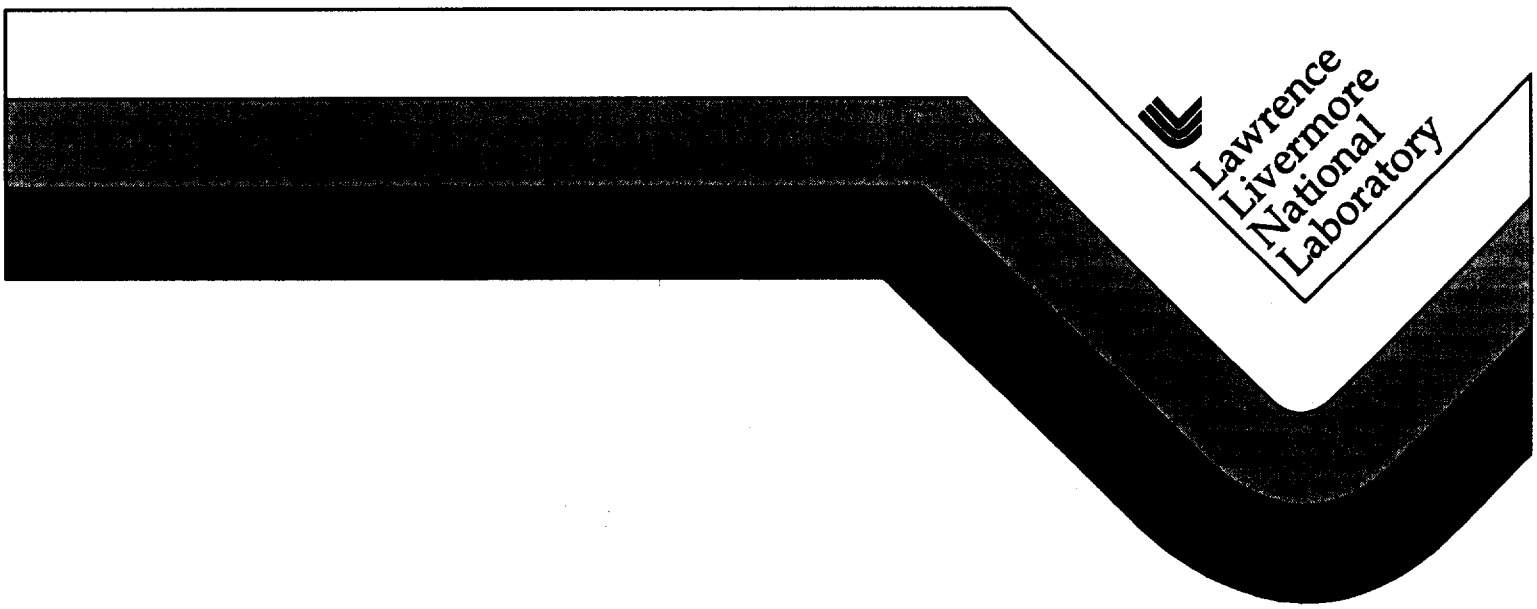

DISCLAIMER

This document was prepared as an account of work sponsored by an agency of the United States Government. Neither the United States Government nor the University of California nor any of their employees, makes any warranty, express or implied, or assumes any legal liability or responsibility for the accuracy, completeness, or usefulness of any information, apparatus, product, or process disclosed, or represents that its use would not infringe privately owned rights. Reference herein to any specific commercial product, process, or service by trade name, trademark, manufacturer, or otherwise, does not necessarily constitute or imply its endorsement, recommendation, or favoring by the United States Government or the University of California. The views and opinions of authors expressed herein do not necessarily state or reflect those of the United States Government or the University of California, and shall not be used for advertising or product endorsement purposes.

Work performed under the auspices of the U.S. Department of Energy by Lawrence Livermore National Laboratory under Contract W-7405-ENG-48.

# Final Report to LLNL: IUT Agreement B264110
# Solution of Dynamic Contact Problems
# by Implicit/Explicit Methods

by
Matthew W. Salveson
and
Robert L. Taylor
Department of Civil and Environmental Engineering
University of California, Berkeley

## Executive Summary

The solution of dynamic contact problems within an explicit finite element program such as the LLNL *DYNA* programs is addressed in the attached report. Our approach is to represent the solution for the deformation of bodies using the explicit algorithm but to solve the contact part of the problem using an *implicit* approach. Thus, the contact conditions at the next solution state are considered when computing the acceleration state for each explicit time step. For the current development we employ a Newmark update procedure where the position of a node at the next step is given by

$$\boldsymbol{x}_{n+1} = \boldsymbol{x}_n + \Delta t \boldsymbol{v}_n + \frac{1}{2}\Delta t^2 \boldsymbol{a}_n$$

A *normal gap* for each slave node to master segment is computed using interpolants of the above Newmark formula. For normal gaps which violate the impenetrability condition for solid bodies a node to segment contact constraint is introduced. This leads to a set of equations which couple the degrees of freedom which, when linearized, lead to a set of simultaneous linear equations. Thus, the contact part is implicit.

Since the explicit time step is constrained by the Courant condition, we assume that changes in the directions of the normal to contact surfaces do not change rapidly. Using this constraint, the gap condition becomes linear and it is necessary to only solve the implicit equations once per time step.

For contact conditions which are node-node we are able to show that satisfying the contact conditions using the above approach lead to states for which the velocities and accelerations computed from the Newark formulas are free from spurious jumps commonly encountered in explicit solutions. The interpolated conditions may not satisfy the jump states exactly, but numerical solutions confirm that good results are obtained. To facilitate the description of contact surfaces an automatic enumeration for the slave nodes and master segments on the surfaces of each body was employed.

The drawback of the method proposed in the study is the need to solve the implicit set of equations resulting from contacts. This is offset by the improved velocity/acceleration states obtained and the fact that no reduction in the Courant condition for setting the time step is imposed by contacts. While our study employed a direct solution for the linear implicit solutions resulting from contacts an iterative scheme, e.g., a preconditioned conjugate gradient method, may be employed.

# *An Explicit-Implicit Contact Algorithm*

MATTHEW W. SALVESON
Department of Civil Engineering
University of California, Berkeley, CA 94720

*Written Under The Supervision of:*

ROBERT L. TAYLOR
Department of Civil Engineering
University of California, Berkeley, CA 94720

## 1. ABSTRACT

This paper addresses the solution of dynamic contact problems by finite element methods. A new treatment for transient effects associated with initial dynamical contacts between two bodies is developed and implemented. For many treatments, it is necessary to introduce an artificial dissipation mechanism into an analysis to control oscillations resulting from the impacts associated with dynamical contacts. For an explicit algorithm, it is possible to introduce the constraints on the displacement field such that the spurious oscillations may be avoided without using artificial damping. The proposed treatment uses an explicit-implicit algorithm in which an explicit predictor step is performed. In the case of contact, an implicit corrector step is then performed that enforces the zero gap constraint at all points of contact. This algorithm minimizes the spurious oscillations usually associated with dynamic contact problems.

## 2. INTRODUCTION

The analysis of interacting bodies which include the effects of both material nonlinearity and large deformations has received considerable attention during the last few years[2-11, 13-21, 23-38]. Many improvements to this type of analysis have been made and it is possible to effectively address a class of nonlinear systems

in which constraints that reflect contact are included. In most work reported to date, one-step methods have been used to advance the solution in time. General classes of one-step methods have been proposed for the time integration of the momentum balance equation by many authors, including Newmark[22] and Katona and Zienkiewicz[12].

Much effort has been expended to develop stable and accurate methods which may be applied to general classes of problems. In general, methods are divided into groups: (1) explicit integration of the momentum balance equations; and (2) implicit integration of the momentum balance equations. In this paper a study is presented to consider a general treatment of contact constraints and their effects on a transient analysis. Special consideration is directed to the dynamical aspects of contact problems so that use of artificial diffusion mechanisms may be avoided.

Section 3 of this report develops the contact equations for a general hyperelastic material. Section 4 develops the dynamic equations of motion. Section 5 examines the behavior of the velocity and acceleration fields at contact interfaces. Section 6 presents a 2-D contact detection algorithm. Section 7 presents a number of examples that test the proposed algorithm.

## 3. DEVELOPMENT OF VARIATIONAL EQUATIONS

This section develops the contact equations for a general hyperelastic material.

Consider a body **B** occupying a region $\Omega_t$ with boundary $\partial\Omega_t$ at some time $t$. Define the region occupied by **B** at time $t_0$ to be $\Omega_0$, the reference configuration, with boundary $\partial\Omega_0$. Each material point in the body is represented by its position vector **X** in the reference configuration. Assume the existence of an invertible mapping $\boldsymbol{\phi} : \Omega_0 \times \Re \rightarrow \Omega_t$ such that

$$\mathbf{x} = \boldsymbol{\phi}(\mathbf{X}, t) \tag{3.1}$$

where **x** is the position vector of the material point **X** in the current configuration $\Omega_t$. See Figure 3.1.

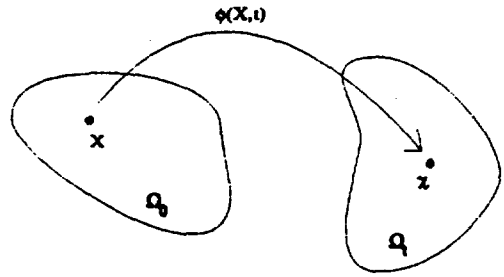


**FIGURE 3.1** Mapping of Reference Configuration to Current Configuration

A fundamental measure of deformation is the deformation gradient defined by

$$\mathbf{F} = \frac{\partial \boldsymbol{\phi}}{\partial \mathbf{X}} = \nabla_0 \boldsymbol{\phi} \tag{3.2}$$

from which the first Piola-Kirchoff stress tensor for finite elasticity may be deduced from an energy functional $W$:

$$\mathbf{P} = \rho_0 \frac{\partial \widehat{W}(\mathbf{F})}{\partial \mathbf{F}} \tag{3.3}$$

where

$$W = \tilde{W}(\nabla_0 \mathbf{u}) = \widehat{W}(\mathbf{F}) \tag{3.4}$$

It is common in numerical simulations to introduce the displacement field (assuming a constant basis $\mathbf{e}_i$ and common origin for the body)

$$\mathbf{u} = \mathbf{x} - \mathbf{X} \tag{3.5}$$

Hence,

$$\nabla_0 \mathbf{u} = \mathbf{F} - \mathbf{I} \tag{3.6}$$

This gives

$$\mathbf{P} = \rho_0 \frac{\partial \tilde{W}(\nabla_0 \mathbf{u})}{\partial(\nabla_0 \mathbf{u})} \tag{3.7}$$

Consider a body force per unit mass in the reference configuration, $\mathbf{b}_0$, and a surface traction $\mathbf{p}$ defined by $\mathbf{p} = \mathbf{PN}$ where $\mathbf{N}$ is the outward normal to the surface in the reference configuration. These terms together with $W$ may be used to express the energy functional $\Pi(\mathbf{u})$:

$$\Pi(\mathbf{u}) = \int_{\Omega_0} \rho_0 \tilde{W}(\nabla_0 \mathbf{u})\, dV - \int_{\Omega_0} \rho_0 \mathbf{b}_0 \cdot \mathbf{u}\, dV - \int_{\partial\Omega_0} \mathbf{p}_0 \cdot \mathbf{u}\, dA \tag{3.8}$$

We desire a valid solution for $\mathbf{u}$ such that

$$\delta\Pi(\mathbf{u}) = \int_{\Omega_0} \mathbf{P} \cdot \nabla_0(\delta\mathbf{u})\, dV - \int_{\Omega_0} \rho_0 \mathbf{b}_0 \cdot \delta\mathbf{u}\, dV - \int_{\partial\Omega_0} \mathbf{p} \cdot \delta\mathbf{u}\, dA = 0 \tag{3.9}$$

This may now be transformed to the current configuration to yield

$$\int_{\Omega_t} \boldsymbol{\sigma} \cdot \nabla(\delta\mathbf{u})\, dv - \int_{\Omega_t} \rho \mathbf{b} \cdot \delta\mathbf{u}\, dv - \int_{\partial\Omega_t} \mathbf{p} \cdot \delta\mathbf{u}\, da = 0 \tag{3.10}$$

where

$$\begin{aligned} \mathbf{t} &= \boldsymbol{\sigma}\mathbf{n} \\ \boldsymbol{\sigma} &= \frac{1}{J}\mathbf{P}\mathbf{F}^T \\ J &= det(\mathbf{F}) \end{aligned} \tag{3.11}$$

Here, $\mathbf{n}$ is the outward unit normal to the surface in the current configuration.

Utilizing D'Alembert's principle, Equation (3.10) may now be modified to include inertial terms:

$$\int_{\Omega_t} \boldsymbol{\sigma} \cdot \nabla(\delta\mathbf{u})\, dv + \int_{\Omega_t} \rho\ddot{\mathbf{u}}\, dv - \int_{\Omega_t} \rho \mathbf{b} \cdot \delta\mathbf{u}\, dv - \int_{\partial\Omega_t} \mathbf{p} \cdot \delta\mathbf{u}\, da = 0 \tag{3.12}$$

Once an expression for $W$ is chosen, a stress function may be computed:

$$\boldsymbol{\sigma} = \mathbf{f}(\nabla_0 \mathbf{u}) \tag{3.13}$$

Spatial discretization of the body $\mathbf{B}$ using finite element methods [39, 40] will then yield the familiar equations

$$\mathbf{M}\ddot{\mathbf{u}} + \mathbf{P}(\mathbf{u}) = \mathbf{F} \tag{3.14}$$

To include the effects of contact, Equation (3.8) is augmented with a set of constraints, $\mathbf{g}$, and their Lagrange multipliers, $\boldsymbol{\lambda}$ :

$$\hat{\Pi}(\mathbf{u}, \boldsymbol{\lambda}) = \Pi(\mathbf{u}) + \boldsymbol{\lambda} \cdot \mathbf{g} \tag{3.15}$$

$\mathbf{g}$ is the $n_{t\lambda}$ order vector describing $n$ discrete constraints on the displacement field. Here, each constraint is a zero penetration condition at the discrete points of contact.

Define the second term on the right hand side of Equation (3.15) as

$$\Pi_{con} = \boldsymbol{\lambda} \cdot \mathbf{g} \tag{3.16}$$

The first variation of Equation (3.16) is

$$\delta\Pi_{con} = \delta\boldsymbol{\lambda} \cdot \mathbf{g} + \boldsymbol{\lambda} \cdot \delta\mathbf{g} = \delta\boldsymbol{\lambda} \cdot \mathbf{g} + \left(\frac{\partial \mathbf{g}}{\partial \mathbf{u}}\delta\mathbf{u}\right) \cdot \boldsymbol{\lambda} = \delta\boldsymbol{\lambda} \cdot \mathbf{g} + \delta\mathbf{u} \cdot (\mathbf{G}(\mathbf{u})\boldsymbol{\lambda}) \tag{3.17}$$

where

$$\mathbf{G}(\mathbf{u}) = \left(\frac{\partial \mathbf{g}}{\partial \mathbf{u}}\right)^T \tag{3.18}$$

A point of contact between a slave node, $\mathbf{m}_s$, on a slave surface, and a master surface defined by the line between Master Node 1, $\mathbf{m}_1$, and Master Node 2, $\mathbf{m}_2$, is diagrammed below in Figure 3.2.

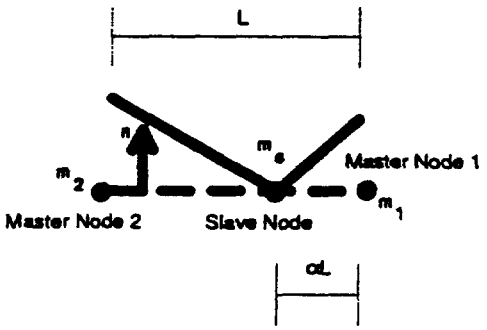


**FIGURE 3.2** Discrete Point of Contact

For the moment, we will assume that the normal is constant along the master segment. Note that this contact condition may exist between two distinct bodies or two points on a single body.

At time $t_{n+1}$ the gap condition at point $i$ is defined by

$$g_i = (\mathbf{x}_{ms} - (1-\alpha^i)\mathbf{x}_{m1} - \alpha^i\mathbf{x}_{m2}) \cdot \mathbf{n} \tag{3.19}$$

where for the $i_{th}$ gap condition

$$\begin{aligned} \mathbf{x}_{ms} &= \mathbf{A}^i_{ms}\mathbf{x} \\ \mathbf{x}_{m1} &= \mathbf{A}^i_{m1}\mathbf{x} \\ \mathbf{x}_{m2} &= \mathbf{A}^i_{m2}\mathbf{x} \end{aligned} \tag{3.20}$$

where **A** is a Boolean selection operator.

Noting that $\delta\mathbf{x} = \delta\mathbf{u}$, the first variation of Equation (3.19) becomes

$$\begin{aligned} \delta g_i =& (\mathbf{A}^i_{ms} - (1-\alpha^i)\mathbf{A}^i_{m1} - \alpha^i\mathbf{A}^i_{m2})\delta\mathbf{u} \cdot \mathbf{n} + \\ & (\delta\alpha^i(\mathbf{A}^i_{m1} - \mathbf{A}^i_{m2})\mathbf{x}) \cdot \mathbf{n} + \\ & ((\mathbf{A}^i_{ms} - (1-\alpha^i)\mathbf{A}^i_{m1} - \alpha^i\mathbf{A}^i_{m2})\mathbf{x}) \cdot \delta\mathbf{n} \end{aligned} \tag{3.21}$$

This may be written as

$$\begin{aligned}\delta g_i =&(\mathbf{A}^i_{ms} - (1-\alpha^i)\mathbf{A}^i_{m1} - \alpha^i\mathbf{A}^i_{m2})\delta\mathbf{u}\cdot\mathbf{n}+\\ &(\mathbf{A}^i_\alpha\delta\mathbf{u})\cdot\left(\frac{\mathbf{A}^i_\alpha\mathbf{x}}{\|\mathbf{A}^i_\alpha\|\mathbf{x}}\right)((\mathbf{A}^i_{m1}-\mathbf{A}^i_{m2})\mathbf{x})\cdot\mathbf{n}+\\ &(\mathbf{T}\cdot(\mathbf{B}^i\delta\mathbf{u}))\left(\frac{1}{\|\mathbf{N}\|^3}\right)((\mathbf{A}^i_{ms}-(1-\alpha^i)\mathbf{A}^i_{m1}-\alpha^i\mathbf{A}^i_{m2})\mathbf{x})\cdot\mathbf{T}\end{aligned} \tag{3.22}$$

Equation (3.22) may be generalized to the case where a continuous outward normal is interpolated along the master contact segment.

Setting the first variation of Equation (3.15) to zero yields at time $t_{n+1}$

$$\begin{aligned}&\mathbf{M}_{n+1}\ddot{\mathbf{u}}_{n+1} + \mathbf{P}(\mathbf{u}_{n+1}) + \mathbf{G}(\mathbf{u}_{n+1})\boldsymbol{\lambda}_{n+1} = \mathbf{F}^{ext}_{n+1}\\ &\mathbf{g}_{n+1} = \mathbf{0}\end{aligned} \tag{3.23}$$

where at time $t_{n+1}$

$$\begin{aligned}&\mathbf{M}_{n+1} \text{ is the mass matrix}\\ &\mathbf{P}(\mathbf{u}_{n+1}) \text{ is the stress divergence}\\ &\mathbf{G}(\mathbf{u}_{n+1}) \text{ is the contact matrix}\\ &\mathbf{F}^{ext}_{n+1} \text{ is the vector of external loads}\\ &\mathbf{g}_{n+1} \text{ is the vector of constraints}\end{aligned} \tag{3.24}$$

Equation ($3.23_1$) is a set of ordinary differential equations and Equation ($3.23_2$) is a set of algebraic equations. The pair together is known as differential algebraic equations (DAE) [1] and may be conveniently solved using one-step time integration methods. For example, using the Newmark method [22] we have

$$\begin{aligned}\mathbf{u}_{n+1} &= \mathbf{u}_n + \Delta t_n\mathbf{v}_n + (\Delta t_n)^2(\frac{1}{2}-\beta)\mathbf{a}_n + (\Delta t_n)^2\beta\mathbf{a}_{n+1}\\ \mathbf{v}_{n+1} &= \mathbf{v}_n + \Delta t_n(1-\gamma)\mathbf{a}_n + \Delta t_n\gamma\mathbf{a}_{n+1}\end{aligned} \tag{3.25}$$

where

$$\begin{aligned}\Delta t_n &= t_{n+1} - t_n\\ \mathbf{v}_n &= \dot{\mathbf{u}}_n\\ \mathbf{a}_n &= \ddot{\mathbf{u}}_n\\ \beta,\gamma &= \text{ integration constants}\end{aligned} \tag{3.26}$$

For non-zero $\beta$ and $\gamma$ , Equation (3.23) may now, in general, be solved. However, for the explicit algorithm with $\beta = 0.0$ and $\gamma = 0.5$, Equation (3.23) is modified to

$$\begin{aligned}&\mathbf{M}_{n+1}\ddot{\mathbf{u}}_{n+1} + \mathbf{G}(\mathbf{u}_{n+1})\boldsymbol{\lambda}_{n+1} = \mathbf{F}^{ext}_{n+1} - \mathbf{P}(\mathbf{u}_{n+1})\\ &\mathbf{g}_{n+2} = \mathbf{0}\end{aligned} \tag{3.27}$$

Note that the gap condition is now to be satisfied at time $t_{n+2}$. This is because for explicit time integration, the displacement field at time $t_{n+2}$ is entirely defined by the state at time $t_{n+1}$. We then choose the rate terms at time $t_{n+1}$ to satisfy the gap constraints at time $t_{n+2}$.

To facilitate solution of the contact terms in Equation (3.27), a number of simplifying assumptions will be made as discussed in the next section.

## 4. EQUATIONS OF MOTION

For our algorithm, we neglect the second and third term in Equation (3.21). The first term is O(1). The second term is $O(\Delta t^2)$, so it is neglected. The third term is neglected because the outward normal n is assumed to be constant between the predictor and corrector step (this is the only step when contact is considered). This assumption is acceptable only because this algorithm is subject to the numerical stability constraints of an explicit algorithm.

An explicit algorithm for a linear elastic material requires that

$$\Delta t \leq \frac{h}{c_{max}} \tag{4.1}$$

whee $h$ is a characteristic length and $c_{max}$ is the maximum wave speed in the material.

Significant errors in the calculation of the normal can only be introduced if the velocity of contact segment approaches the natural wave speeds of the materials.

Assuming that n is constant between the predictor step and the corrector step makes Equation (3.21) linear in u. For clarity we rewrite Equation (3.27), noting this linearity

$$\begin{aligned} &\mathbf{M}_{n+1}\ddot{\mathbf{u}}_{n+1} + \mathbf{G}_{n+1}\boldsymbol{\lambda}_{n+1} = \mathbf{F}^{ext}_{n+1} - \mathbf{P}(\mathbf{u}_{n+1}) \\ &\mathbf{g}_{n+2} = \mathbf{0} \end{aligned} \tag{4.2}$$

We now assume that the mass represented by $\mathbf{M}_{n+1}$ is lumped at the nodes. Because the forces, $\boldsymbol{\lambda}_{n+1}$, are not initially known, the following predictor equations are solved explicitly:

$$\mathbf{M}\bar{\mathbf{a}}_{n+1} = \mathbf{F}^{ext}_{n+1} - \mathbf{P}(\mathbf{u}_{n+1}) \tag{4.3}$$

Velocity and position "predictor" terms are then found using the explicit Newmark discretization.

$$\begin{aligned} \bar{\mathbf{v}}_{n+1} &= \mathbf{v}_n + \frac{1}{2}\Delta t_n(\mathbf{a}_n + \bar{\mathbf{a}}_{n+1}) \\ \bar{\mathbf{x}}_{n+2} &= \mathbf{x}_{n+1} + \Delta t_{n+1}\bar{\mathbf{v}}_{n+1} + \frac{1}{2}(\Delta t_{n+1})^2\bar{\mathbf{a}}_{n+1} \end{aligned} \tag{4.4}$$

Equilibrium must be enforced at time $t_{n+1}$ and the zero penetration condition must be enforced at time $t_{n+2}$.

$\mathbf{n}_{n+2}$ and $\mathbf{g}_{n+2}$ are certainly not known *a priori*, but may be approximated using the "predictor" positions of the master and slave nodes. Additionally, iteration on the contact (or "corrector") stage of this algorithm may be used to yield better values for both $\mathbf{n}_{n+2}$ and $\mathbf{g}_{n+2}$.

Note that if the $i_{th}$ gap condition, $g^i$, is greater then zero for the "predictor" values of position, velocity, and acceleration are correct and no contact has taken place at the $i_{th}$ point during this time step. If contact has occurred, $g^i$ must be set to zero and position, velocity, and acceleration terms must be "corrected" to account for the external contact forces on the bodies. This is done by subtracting Equation (4.3) from Equation (4.2).

$$\begin{aligned} &\mathbf{M}(\mathbf{a}_{n+1} - \bar{\mathbf{a}}_{n+1}) + \mathbf{G}_{n+1}\boldsymbol{\lambda} = \mathbf{0} \\ &\mathbf{g}_{n+2} = \mathbf{0} \end{aligned} \tag{4.5}$$

Equation (4.5) may be expressed as the symmetric system of linear equations

$$\begin{bmatrix} \mathbf{M} & \mathbf{G}_{n+1} \\ \mathbf{G}^T_{n+1} & \mathbf{0} \end{bmatrix} \cdot \begin{bmatrix} \mathbf{a}_{n+1} \\ \boldsymbol{\lambda}_{n+1} \end{bmatrix} = \begin{bmatrix} \mathbf{R}_1 \\ \mathbf{R}_2 \end{bmatrix} \tag{4.6}$$

where

$$\mathbf{R}_1 = \mathbf{M}\bar{\mathbf{a}}_{n+1}$$
$$\mathbf{R}_2 = -\mathbf{G}_{n+1}^T \left( \mathbf{x}_{n+1} + \Delta t_{n+1} \left( \mathbf{v}_n + \frac{1}{2}\Delta t_n \mathbf{a}_n \right) \right) \frac{2}{(\Delta t_{n+1})^2 + \Delta t_{n+1}\Delta t_n} \tag{4.7}$$

Once Equation (4.6) is solved for $\mathbf{a}_{n+1}$, corrected values for $\mathbf{v}_{n+1}$ and $\mathbf{x}_{n+2}$ may then be obtained using the Newmark integration scheme.

## 5. BEHAVIOR OF INTERFACE VELOCITY AND ACCELERATION

In the previous section, we motivate the imposition of a gap constraint on the displacement field at time $t_{n+2}$. This leads to other desirable properties.

An implicit Newmark time integration algorithm will lead to spurious results in the velocity and acceleration fields if the zero gap condition is only imposed on the displacement field. This is not the case for an explicit Newmark time integration algorithm. All spurious results on the velocity and acceleration fields vanish after two time steps.

The Newmark temporal discretization is given by

$$\begin{aligned} \mathbf{v}_{n+1} &= \mathbf{v}_n + \Delta t_n(1-\gamma)\mathbf{a}_{n+1} \\ \mathbf{x}_{n+2} &= \mathbf{x}_{n+1} + \Delta t_{n+1}\mathbf{v}_{n+1} + \frac{1}{2}(\Delta t_{n+1})^2(1-\beta)\mathbf{a}_{n+1} + \frac{1}{2}(\Delta t_n)^2\beta\mathbf{a}_{n+2} \\ \Delta t_{n+i} &= t_{n+i+1} - t_{n+i} \end{aligned} \tag{5.1}$$

For an explicit algorithm, choose $\beta = 0.0$ and $\gamma = 0.5$. Assume the zero gap condition is enforced on the displacement field at times $t_{n+2}$, $t_{n+3}$, and $t_{n+4}$, such that for a one dimensional problem

$$\begin{aligned} \mathbf{x}_{n+2}^s &= \mathbf{x}_{n+2}^m \\ \mathbf{x}_{n+3}^s &= \mathbf{x}_{n+3}^m \\ \mathbf{x}_{n+4}^s &= \mathbf{x}_{n+4}^m \end{aligned} \tag{5.2}$$

Consider the zero gap condition at time $t_{n+4}$. Equation (5.1) gives us

$$\mathbf{x}_{n+3}^s + \Delta t_{n+3}\mathbf{v}_{n+3}^s + \frac{1}{2}(\Delta t_{n+3})^2\mathbf{a}_{n+3}^s = \mathbf{x}_{n+3}^m + \Delta t_{n+3}\mathbf{v}_{n+3}^m + \frac{1}{2}(\Delta t_{n+3})^2\mathbf{a}_{n+3}^m \tag{5.3}$$

Noting that the zero gap condition is also satisfied at time $t_{n+3}$

$$\mathbf{v}_{n+3}^s + \frac{1}{2}\Delta t_{n+3}\mathbf{a}_{n+3}^s = \mathbf{v}_{n+3}^m + \frac{1}{2}\Delta t_{n+3}\mathbf{a}_{n+3}^m \tag{5.4}$$

Equation ($5.1_1$) may be substituted into Equation (5.4) to give

$$\begin{aligned} &\mathbf{v}_{n+2}^s + \frac{1}{2}\Delta t_{n+2}\mathbf{a}_{n+2}^s + \frac{1}{2}(\Delta t_{n+2}\Delta t_{n+3})\mathbf{a}_{n+2}^s = \\ &\mathbf{v}_{n+2}^m + \frac{1}{2}\Delta t_{n+2}\mathbf{a}_{n+2}^m + \frac{1}{2}(\Delta t_{n+2}\Delta t_{n+3})\mathbf{a}_{n+2}^m \end{aligned} \tag{5.5}$$

Similarily, the zero gap condition at times $t_{n+2}$ and $t_{n+3}$ yields

$$\mathbf{v}_{n+2}^s + \frac{1}{2}\Delta t_{n+2}\mathbf{a}_{n+2}^s = \mathbf{v}_{n+2}^m + \frac{1}{2}\Delta t_{n+2}\mathbf{a}_{n+2}^m \tag{5.6}$$

Substitution into Equation (5.5) gives

$$\mathbf{a}_{n+3}^s = \mathbf{a}_{n+3}^m \tag{5.7}$$

Substituting this into Equation (5.4) gives

$$\mathbf{v}^s_{n+3} = \mathbf{v}^m_{n+3} \tag{5.8}$$

Note that for persistent contact, enforcement of the zero gap condition on the displacement field will also produce a zero gap condition on the velocity and acceleration fields for all time points greater then or equal to $t_{n+3}$.

For two or more dimensions, define an outward surface normal at time $t_i$ to be $\mathbf{n}_i$. Assume the zero gap condition is enforced on the displacement field at times $t_{n+2}$, $t_{n+3}$, and $t_{n+4}$, such that

$$\begin{aligned}&(\mathbf{x}^s_{n+2} - \mathbf{x}^m_{n+2}) \cdot \mathbf{n}_{n+2}\\ &(\mathbf{x}^s_{n+3} - \mathbf{x}^m_{n+3}) \cdot \mathbf{n}_{n+3}\\ &(\mathbf{x}^s_{n+4} - \mathbf{x}^m_{n+4}) \cdot \mathbf{n}_{n+4}\end{aligned} \tag{5.9}$$

Proceeding in a similar manner as before will yield

$$\begin{aligned}&(\mathbf{x}^s_{n+3} - \mathbf{x}^m_{n+3}) \cdot (\mathbf{n}_{n+4} - \mathbf{n}_{n+3}) +\\ &\frac{1}{2}\Delta t_{n+2}(\Delta t_{n+2} + \Delta t_{n+3})(\mathbf{a}^s_{n+3} - \mathbf{a}^m_{n+3}) \cdot \mathbf{n}_{n+3} -\\ &\frac{\Delta t_{n+3}}{\Delta t_{n+2}}(\mathbf{x}^s_{n+2} - \mathbf{x}^m_{n+2}) \cdot (\mathbf{n}_{n+3} - \mathbf{n}_{n+2}) +\\ &\Delta t_{n+3}\left[\left(\mathbf{v}^s_{n+2} + \frac{1}{2}\Delta t_{n+2}\mathbf{a}^s_{n+2}\right) - \left(\mathbf{v}^m_{n+2} + \frac{1}{2}\Delta t_{n+2}\mathbf{a}^m_{n+2}\right)\right] \cdot (\mathbf{n}_{n+4} - \mathbf{n}_{n+4}) = 0\end{aligned} \tag{5.10}$$

If we assume that the rotation of a contact surface is relatively small between time steps then we may assume

$$\mathbf{n}_{n+2} \approx \mathbf{n}_{n+3} \approx \mathbf{n}_{n+2} \tag{5.11}$$

Which then leads to the desired result

$$\begin{aligned}&(\mathbf{a}^s_{n+3} - \mathbf{a}^m_{n+3}) \cdot \mathbf{n}_{n+3}\\ &(\mathbf{v}^s_{n+3} - \mathbf{v}^m_{n+3}) \cdot \mathbf{n}_{n+3}\end{aligned} \tag{5.12}$$

The explicit-implicit algorithm proposed in this report will preserve this behavior of the velocity and acceleration fields across the contact interface.

## 6. A 2-D CONTACT DETECTION ALGORITHM

This algorithm assumes a peicewise linear contact surface. It assumes a constant velocity during the current time step. It will produce a normalized time of contact, $\tau_c$, as well as the point of contact, $\alpha$. See Figure 6.1, Figure 6.2, and Figure 6.3.

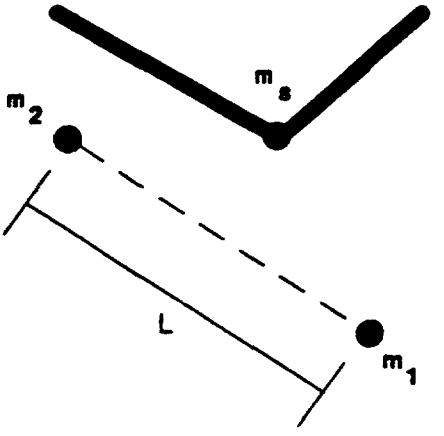


**FIGURE 6.1** Contact Point $\tau = 0$

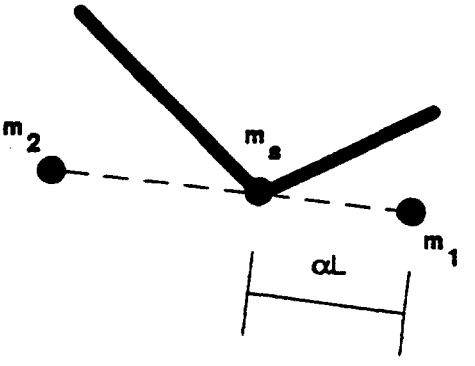


**FIGURE 6.2** Contact Point $\tau = \tau_c$

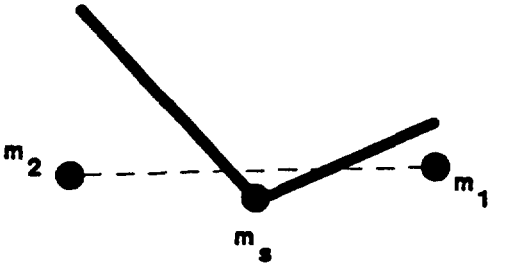


**FIGURE 6.3** Contact Point $\tau = 1$

Define $\mathbf{xs}_i$, $\mathbf{xm1}_i$, and $\mathbf{xm2}_i$ to be the position vectors at $\tau = 0$ for the slave node, master node 1, and master node 2, respectively. Also, define $\mathbf{xs}_f$, $\mathbf{xm1}_f$, and $\mathbf{xm2}_f$ to be the position vectors at $\tau = 1$ for the slave node, master node 1, and master node 2, respectively. For contact detection we assume constant velocity within each time step, thus these position vectors may be expressed as a linear function of $\tau$.

$$\begin{aligned} \mathbf{xs} &= \mathbf{xs}_i(1-\tau) + \mathbf{xs}_f\tau \\ \mathbf{xm1} &= \mathbf{xm1}_i(1-\tau) + \mathbf{xm1}_f\tau \\ \mathbf{xm2} &= \mathbf{xm2}_i(1-\tau) + \mathbf{xm2}_f\tau \end{aligned} \tag{6.1}$$

The normal is constant along the length of the master element. It may also be defined as a function of $\tau$.

$$\begin{aligned}
\mathbf{n} &= \mathbf{n}_i(1-\tau) + \mathbf{n}_f\tau \\
\mathbf{N}_i &= (\mathbf{xm2}_i - \mathbf{xm1}_i) \times \mathbf{e}_3 \\
\mathbf{n}_i &= \frac{\mathbf{N}_i}{\|\mathbf{N}_i\|} \\
\mathbf{N}_f &= (\mathbf{xm2}_f - \mathbf{xm1}_f) \times \mathbf{e}_3 \\
\mathbf{n}_f &= \frac{\mathbf{N}_f}{\|\mathbf{N}_f\|}
\end{aligned} \tag{6.2}$$

If contact occurs at some $\tau_c$ between $\tau = 0$ and $\tau = 1$, inclusive, then the following must be true:

$$(\mathbf{xs} - \mathbf{xm}_1) \cdot \mathbf{n} \tag{6.3}$$

Substitution of Equation (6.1) and Equation (6.2) into Equation (6.3) will now yield

$$A\tau_c^2 + B\tau_c + C = 0 \tag{6.4}$$

where

$$\begin{aligned}
A &= (\mathbf{n}_f - \mathbf{n}_f) \cdot (-\mathbf{xs}_i + \mathbf{xs}_f + \mathbf{xm1}_f - \mathbf{xm1}_f) \\
B &= \mathbf{n}_i \cdot (-\mathbf{xs}_i + \mathbf{xs}_f + \mathbf{xm1}_f - \mathbf{xm1}_f) + (\mathbf{n}_f - \mathbf{n}_f) \cdot (\mathbf{xs}_i - \mathbf{xm1}_i) \\
C &= \mathbf{n}_i \cdot (\mathbf{xs}_i - \mathbf{xm1}_i)
\end{aligned} \tag{6.5}$$

Once Equation (6.5) is solved for $\tau_c$, $\alpha$ can be found by letting $\tau = \tau_c$.

$$\alpha = \left.\frac{\|\mathbf{xs} - \mathbf{xm1}\|}{\|\mathbf{xm2} - \mathbf{xm1}\|}\right|_{\tau=\tau_c} \tag{6.6}$$

## 7. EXAMPLES

All bodies in the examples are modeled using the non-linear elastic constitutive relation deduced from

$$W(\mathbf{C}) = \frac{1}{2}\lambda(\ln(J))^2 + \mu\left(I_1 - 3 - \frac{1}{2}\ln(J)\right) \tag{7.1}$$

which yields the Cauchy stress-deformation relation:

$$\sigma = \lambda\frac{\ln(J)}{J}\mathbf{1} + \frac{\mu}{J}(\mathbf{b} - \mathbf{1}) \tag{7.2}$$

For small deformations, this model yields results which coincide with isotropic linear elasticity where $\lambda$ and $\mu$ are Lamé constants. For finite deformations, the model gives reasonable results for principal stretches less than 4.0. In examples below, principle stretches are greater than zero and much less than 4.0.

We present a set of example problems which test the performance of the contact formulation presented above. For these calculations we use $\lambda = 33333$ and $\mu = 5000$.

### *7.1. Bar Striking Rigid Surface*

A horizontal bar of dimension 30 by 4 is given an initial velocity of 50. It has an even mesh of 30 by 6 elements. The vertical bar is rigid and fixed in place. It has dimensions of 4 by 30 and has an even mesh of 6 by 30. This mesh is shown in Figure 7.1. Both bars have a mass density of $\rho_0 = 0.1$. Here, however, the vertical bar is rigid and is fixed in place. The horizontal bar is given an initial velocity of 50. The deformed shape is shown in Figure 7.2 with contours for $\sigma_{11}$ superimposed.

This model was compared to one where the horizontal displacements of the tip of the horizontal bar were fixed, yielding identical results.

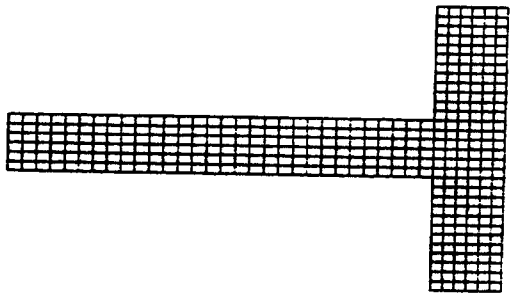

FIGURE 7.1 Bar Striking Rigid Surface, Undeformed Shape

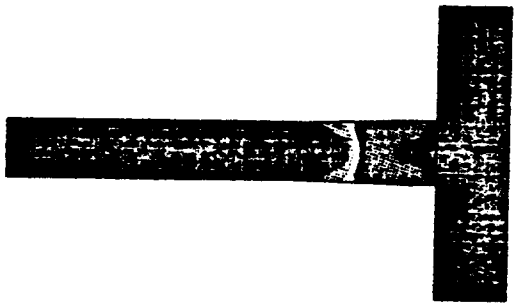

**FIGURE 7.2** Bar Striking Rigid Surface, Deformed Shape, $\sigma_{11}$ Stress

A time history plot of the total energy for the maximum stable time step is show below.

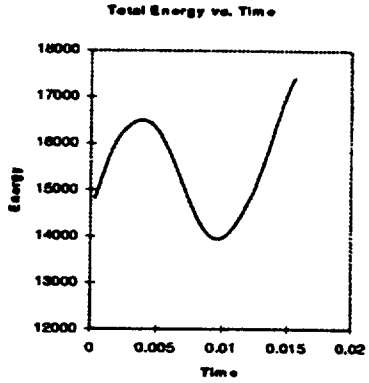


**FIGURE 7.3** Bar Striking Rigid Surface, Total Energy, Maximum Time Step

History plots of tip displacements, velocities and accelerations are given below.

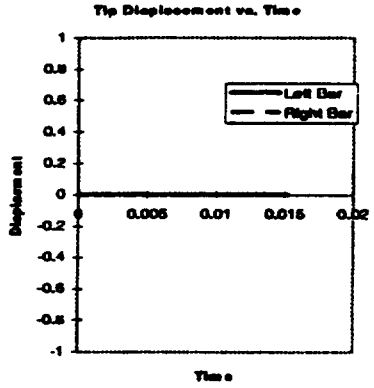


**FIGURE 7.4** Bar Striking Rigid Surface, Tip Displacement

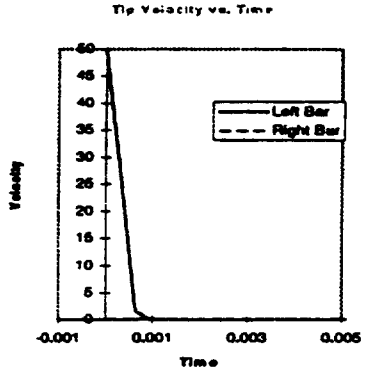


**FIGURE 7.5** Bar Striking Rigid Surface, Tip Velocity

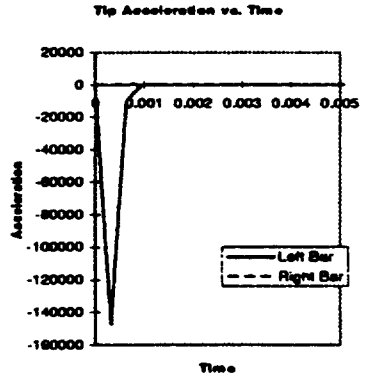


**FIGURE 7.6** Bar Striking Rigid Surface, Tip Acceleration

### *7.2. Bar Striking Compliant Surface*

The undeformed mesh is as before. A horizontal bar of dimension 30 by 4 is given an initial velocity of 50. It has an even mesh of 30 by 6 elements. The vertical bar is unconstrained and initially at rest. It has dimensions 4 by 30 and has an even mesh of 6 by 30. Both bars have a mass density of $\rho_0 = 0.1$.

The deformed shape is shown in Figure 7.7 with contours for $\sigma_{11}$ superimposed.

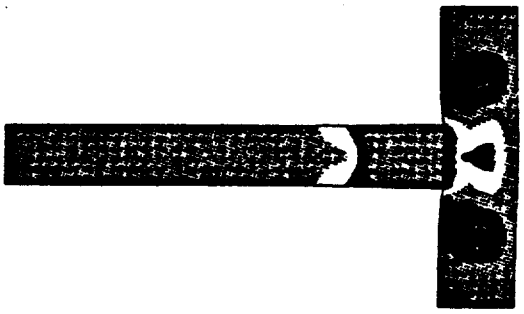

**FIGURE 7.7** Bar Striking Compliant Surface, Deformed Shape, $\sigma_{11}$ Stress

The total energy in the system is calculated at each time step. This time history is shown in Figure 7.8 for a time step that approaches the maximum stable step size for isotropic elasticity. The variations in energy are typical of an explicit solution.

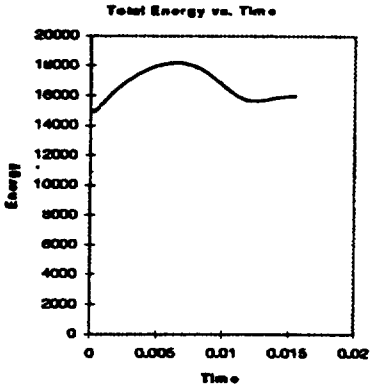


**FIGURE 7.8** Bar Striking Compliant Surface, Total Energy, Maximum Time Step

If the time step is reduced by an order of magnitude, the variation is greatly diminished, as can be seen in Figure 7.9. This behavior is typical for all the examples.

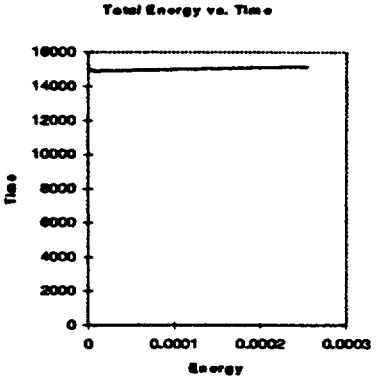


**FIGURE 7.9** Bar Striking Compliant Surface, Total Energy, Small Time Step

Time history plot of tip displacement, velocity and acceleration are given below. Note that there is no high frequency noise. This is because any discontinuous contact behavior is minimized by the explicit-implicit treatment of the contact surface. Any noise is effectively damped out within two time steps. Also note that the zero penetration conditions on the rate terms are not enforced at the instant of contact. The acceleration history exhibits a spike at the point of contact. This spike represents the dirac delta function that is taking

place between two discretized time points. As expected, the velocity and acceleration time histories are self corrected after two time steps.

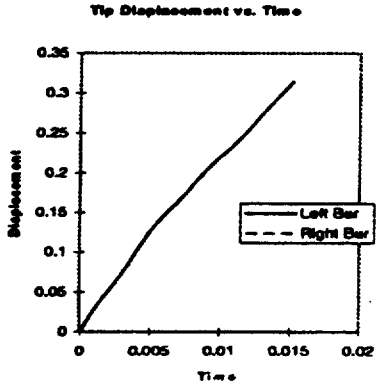


**FIGURE 7.10** Bar Striking Compliant Surface, Tip Displacement

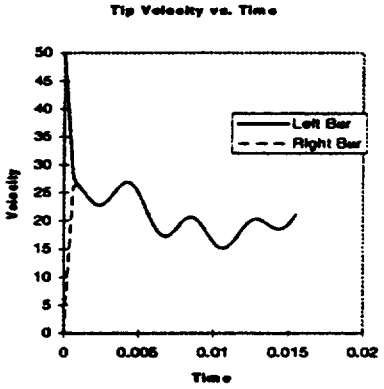


**FIGURE 7.11** Bar Striking Compliant Surface, Tip Velocity

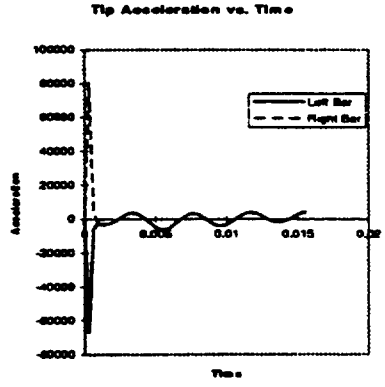


**FIGURE 7.12** Bar Striking Compliant Surface, Tip Acceleration

This example is repeated modifying the mesh of the vertical bar to be 6 by 31. This mesh is shown in Figure 7.13. This will alter the initial contact from node on node on surface. Tip displacements, velocities, and accelerations are then compared to verify that the constraints on these fields still hold. Time histories of these fields are indistinguishable from Figure 7.10, Figure 7.11, and Figure 7.12.

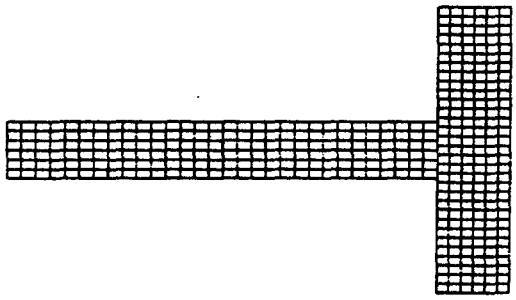

**FIGURE 7.13** Bar Striking Compliant Surface, Undeformed Shape

### *7.3. Bar Striking Like Bar*

Two horizontal bars, both of dimension 30 by 4 are given initial velocities of 50 and -50. Both have an even mesh of 30 by 6 elements. The mesh is shown in Figure 7.14. Both bars have a mass density of $\rho_0 = 0.1$.

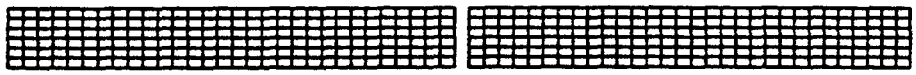

**FIGURE 7.14** Bar Striking Like Bar, Undeformed Shape

The deformed shape is shown in Figure 7.15 with contours for $\sigma_{11}$*superimposed.*

**FIGURE 7.15** Bar Striking Like Bar, Deformed Shape, $\sigma_{11}$*Stress*

Time history plots of tip displacement, tip velocity, and tip acceleration are given below.

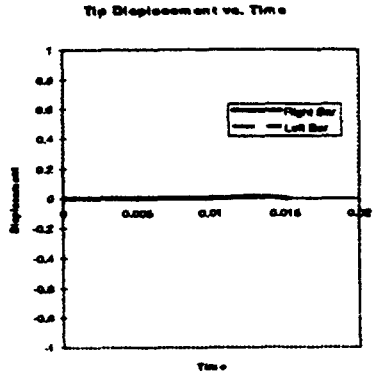


**FIGURE 7.16** Bar Striking Like Bar, Tip Displacement

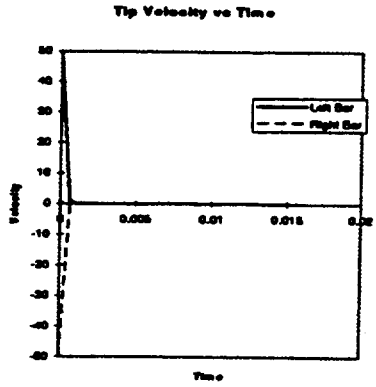


**FIGURE 7.17** Bar Striking Like Bar, Tip Velocity

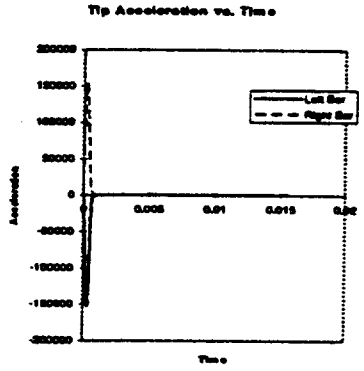


**FIGURE 7.18** Bar Striking Like Bar, Tip Acceleration

*7.4. Bar Striking Dissimilar Bar*

The undeformed mesh is as before. Here, the left bar has a mass density of $\rho_0 = 0.5$ and the right bar has a mass density of $\rho_0 = 1.0$. The deformed mesh is shown in Figure 7.19 with contours for $\sigma_{11}$ superimposed.

**FIGURE 7.19** Bar Striking Unlike Bar, Deformed Shape, $\sigma_{11}$ Stress

Time history plots of tip displacement, tip velocity, and tip acceleration are given below.

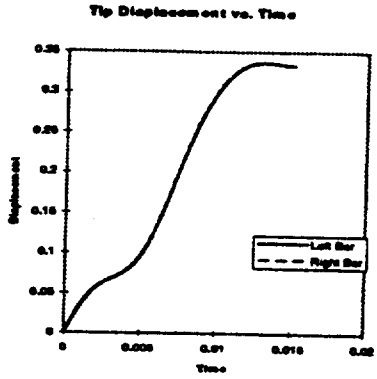

**FIGURE 7.20** Bar Striking Unlike Bar, Tip Displacement

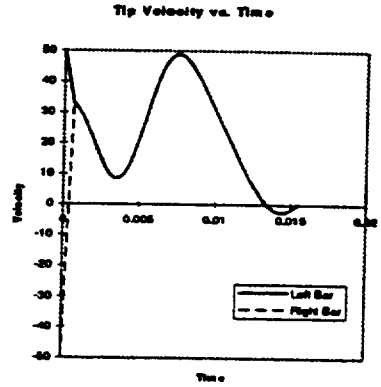

**FIGURE 7.21** Bar Striking Unlike Bar, Tip Velocity

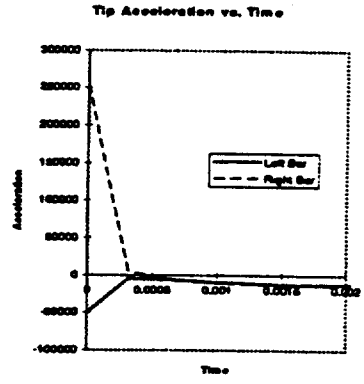

**FIGURE 7.22** Bar Striking Unlike Bar, Tip Acceleration

### *7.5. Disk Striking Compliant Surface*

A disk is given an initial horizontal and vertical velocity. The undeformed mesh is shown in Figure 7.23. A deformed mesh of the disk striking a vertical surface is shown in Figure 7.24. Finally, the disk strikes a horizontal surface in Figure 7.25.

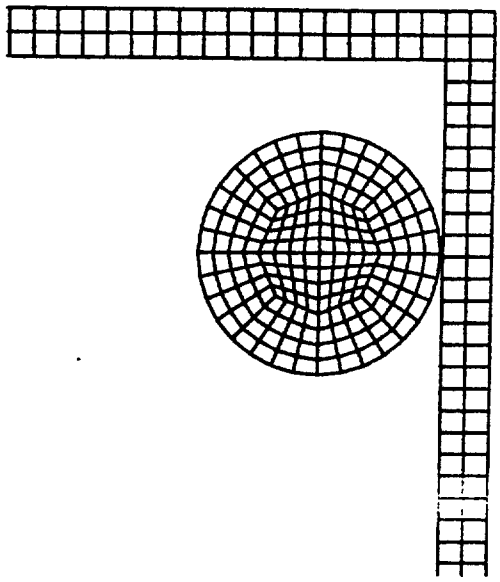

**FIGURE 7.23** Disk Striking Compliant Surface, Undeformed Shape

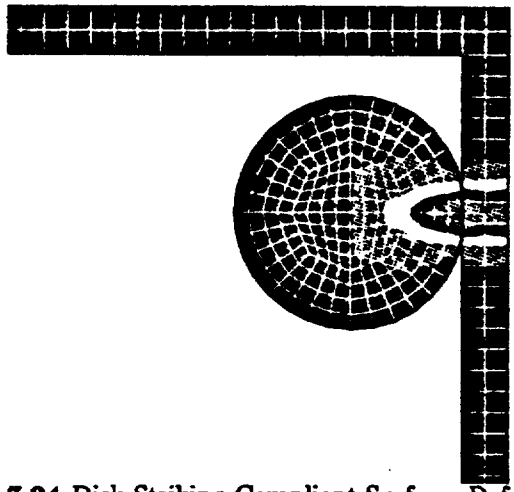

**FIGURE 7.24** Disk Striking Compliant Surface, Deformed Shape, $\sigma_{11}$ Stress

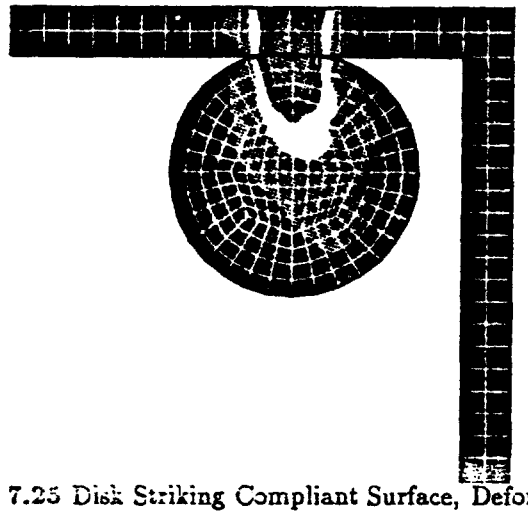

FIGURE 7.25 Disk Striking Compliant Surface, Deformed Shape, $\sigma_{22}$ Stress

## 8. ACKNOWLEDGMENTS

We gratefully acknowlege the financial support for this work kindly provided by the Lawrence Livermore National Laboratory under memorandum agreement B264110.

## 9. REFERENCES

[1] K.E. Brenan, S.L. Campbell, L.R. Petzold, [c1989], *Numerical Solutions of Initial-Value Problems in Differential Algebraic Equations*, North-Holland, New York.

[2] J. Durieu and M. Pettit, [1964], "A 2-D solution of the contact problem in the capstan/tape/roller mechanism of magnetic recorders," *Comp. Meth. Appl. Mech. Engr.*, **43**, 21-35.

[3] T. Endo, J.T. Oden, E.B. Becker and T. Miller, [1984], "A numerical analysis of contact and limit-point behavior in a class of problems of finite elastic deformation," *Comp. and Struct.*, **18**, 899-910.

[4] A. Francavilla and O.C. Zienkiewicz, [1975],"A note on numerical computation of elastic contact problems," *Int. J. Num. Meth. Engr.*, **9**, 913-924.

[5] G.L. Goudreau and J.O. Hallquist, [1982], "Recent developments in large-scale finite element Lagrangian hydrocode technology," *Comp. Meth. Appl. Mech. Engr.*, **33**, 725-757.

[6] F.M. Guerra and R.V. Browning, [1983], "Comparison of two slideline methods using ADINA," *Comp. and Struct.*, **17**, 819-834.

[7] J.O. Hallquist, G.L. Goudreau and D.J. Benson, [1985], "Sliding interfaces with contact-impact in large-scale Lagrangian computations," *Comp. Meth. Appl. Mech. Engr.*, **51**, 107-137.

[8] J.O. HALLQUIST, [1978], "A numerical treatment of sliding interfaces and impact," *ASME AMD-30*, 117-133.

[9] J.O. HUGHES, R.L. TAYLOR, J.L. SACKMAN, A. CURNIER, AND W. KANOKNUKULCHAI, [1976], "A finite element method for a class of contact-impact problems," *Comp. Meth. Appl. Mech. Engr.*, 8, 249-276.

[10] T.J.R. HUGHES, K.S. PISTER, AND R.L. TAYLOR, [1979], "Implicit-explicit finite elements in nonlinear transient analysis," *Comp. Meth. Appl. Mech. Engr.*, 17/18, 159-182.

[11] J.W. JU AND R.L. TAYLOR, [1988], "A perturbed Lagrangian formulation for finite element solution of nonlinear frictional contact problems," *Journal of Theoretical and Applied Mechanics, Special Issue, supplement no. 1 to 7*, 1-14.

[12] M.G. KATONA AND O.C. ZIENKIEWICZ, [1985], "A unified set of single step algorithms, Part 3: the beta-m method, a generalization for the Newmark scheme," *Int. J. Num. Meth. Engr.*, 21, 1345-1359.

[13] N. KIKUCHI AND J.T. ODEN, [1984], "Contact problems in elasto-statics," *Finite Elements: Special Problems in Solid Mechanics*, 5, ed. J.T. Oden and G. Carey, Prentice-Hall, Englewood Cliffs.

[14] N. KIKUCHI, [1982], "A smoothing technique for reduced integration penalty methods in contact problems," *Int. J. Num. Meth. Engr.*, 18, 343-350.

[15] K. KNOTHE AND H.L. THE, [1984], "A contribution to the calculation of the contact stress distribution between two elastic bodies of revulution with non-elliptical contact area," *Comp. and Struct.*, 18, 1025-1033.

[16] J.A. LANDERS AND R.L. TAYLOR, [1985], "An augmented Lagrangian formulation for the finite element solution of contact problems," *SESM Report No. 85/09*, Department of Civil Engineering, University of California, Berkeley.

[17] T.A. LAURSEN AND J.C. SIMO, [1992], "Formulation and regularization of frictinal contact problems with Lagrangian finite element computation," *Proc. 3rd Int. Conf. Computational Plasticity*, (D.R.J. Owen, E. Onate, and E. Hinton, eds.), Pineridge Press, Swansea, U.K., 385-407.

[18] B.C. LEE AND B.M KWAK, [1984], "A computational method for elasto-plastic contact problems," *Comp. and Struct.*, 18, 757-765.

[19] N. MADSEN, [1984], "Numerically efficient procedures for dynamic contact problems," *Int. J. Num. Meth. Engr.*, 20, 1-14.

[20] F.F. MAHMOUD, N.J. SOLAMON AND W.R. MARKS, [1982], "A direct automated procedure for frictionless contact problems," *Int. J. Num. Meth. Engr.*, 18, 245-257.

[21] R. MICHALOWSKI AND Z. MROZ, [1978], "Associated and non-associated sliding rules in contact friction problems," *Archiwum Mechaniki Stosowanej*, 30, 259-276.

[22] N.M. NEWMARK, [1959], "A method of computation for structural dynamics," *J. Engr. Mech. Div.*, ASCE, 67-94.

[23] J.T. ODEN, [1980], "Exterior penalty methods for contact problems in elasticity," *Nonlinear Finite Element Analysis in Structural Mechanics*, ed. K.J. Bathe, E. Stein and W. Wunderlich, Springer Verlag, Berlin.

[24] J.T. ODEN AND J.A.C. MARTINS, [1985], "Models and computational methods for dynamic friction phenomena," *Comp. Meth. Appl. Mech Engr.*, 52, 527-634.

[25] J.T. ODEN AND E.B. PIRES, [1984], "Algorithms and numerical results for finite element approximations of contact problems with non-classical friction laws," *Comp. and Struct.*, 19, 137-147.

[26] J.T. ODEN AND E.B. PIRES, [1983], "Numerical analysis of certain contact problems in elasticity with non-classical friction laws," *Comp. and Struct.*, 16, 481-485.

[27] D. OSMONT, [1982], "Computation of the dynamic response of structures with unilateral constraints (contact) - compared with experimental results," *Comp. Meth. Appl. Mech. Engr.*, 34, 847-859.

[28] P. PAPADOPOULOS, [1991], "On the finite element solution of general contact problems," Ph.D. dissertation, University of California, Berkeley.

[29] E.B. PIRES AND J.T. ODEN, [1983], "Analysis of contact problems with friction under oscillating loads," *Comp. Meth. Appl. Mech. Engr.*, 39, 337-362.

[30] J.C. SIMO, P. WRIGGERS AND R.L. TAYLOR, [1985], "A perturbed Lagrangian formulation for the finite element solution of contact problems," *Comp. Meth. Appl. Mech. Engr.*, 50, 163-180.

[31] E. STEIN AND P. WRIGGERS, [1982], "Calculation of impact-contact problems of thin elastic shells taking into account geometrical nonlinearities within the contact region," *Comp. Meth. Appl. Mech. Engr.*, 34, 861-880.

[32] D. TALASLIDIS AND P.D. PANAGIOTOPOULOS, [1982], "A linear finite element approach to the solution of the variational inequalities arising in contact problems in sturctural dynamics," *Int. J. Num. Meth. Engr.*, 18, 1505-1520.

[33] R.L. TAYLOR AND P. PAPADOPOULOS, [1992], "Finite element solution of dynamics contact problems," Engineering Research, Development and Technology, Lawrence Livermore National Laboratories, *UCRL 53686-91*, 2-42 to 2-46.

[34] J. TSENG AND M.D. OLSON, [1981], "The mixed finite element method applied to two-dimensional elastic contact problems," *Int. J. Num. Meth. Engr.*, 17, 991-1014.

[35] P. WRIGGERS AND J.C. SIMO, [1985], "A note on tangent stiffness for fully nonlinear contact problems," *Commun. Appl. Numer. Meth.*, 1, 199-203, 1985.

[36] P. WRIGGERS, J.C. SIMO AND R.L. TAYLOR, [1985] "Penalty and augmented Lagrangian formulations for contact problems," *Proc. NUMETA 85 Conf.*, Balkema Press, Rotterdam, 97-106.

[37] G. YAGAWA AND H. HIRAYAMA, [1984], "A finite element method for contact problems related to fracture mechanics," *Int. J. Num. Meth. Engr.*, 20, 2175-2195.

[38] ZHONG ZHI-HUA, [1988], "On contact-impact problems," *Linkoping Studies in Science and Technology Dissertation No. 178*, Linkoping University, Sweden.

[39] O.C. ZIENKIEWICZ AND R.L. TAYLOR, [1989], *The Finite Element Method*, 4th ed., Vol 1, McGraw-Hill Book Co., London.

[40] O.C. ZIENKIEWICZ AND R.L. TAYLOR, [1991] *The Finite Element Method*, 4th ed., Vol 2, McGraw-Hill Book Co., London.

[41] O.C. ZIENKIEWICZ, W.L. WOOD, R.L. TAYLOR, [1980], "An alternate single step algorithm for dynamic problems," *Earthquake Engr. and Struct. Dyn.*, 8, 31-40.

[42] O.C. ZIENKIEWICZ, W.L. WOOD, N.W. HINE, R.L. TAYLOR, [1984], "A unified set of single step algorithms, Part 1: general formulation and applications," *Int. J. Num. Meth. Engr.*, 20, 1529-1552.

*Technical Information Department* • **Lawrence Livermore National Laboratory**
**University of California • Livermore, California 94551**